

Supplementary Information

1. General circulation model and drag formulation

The GCM is essentially that described for Jupiter in ref. 1, but with parameters as summarized in Table S1.

TABLE S1: Simulation Parameters

Parameter, symbol	Jupiter	Saturn	Uranus	Neptune
Planetary radius, a (10^6 m)	69.86 ²	57.32 ²	25.27 ³	24.55 ³
Planetary angular velocity, Ω (10^{-4} s)	1.7587 ⁴	1.6388 ³	1.0124 ³	1.0834 ³
Gravitational acceleration, g (m s^{-2})	26.0 ³	10.55 ³	8.94 ³	11.2 ³
Specific gas constant, R ($\text{J kg}^{-1} \text{K}^{-1}$)	3605.38 ³	4016.4 ³	3149.2 ³	3197.7 ³
Adiabatic exponent, κ	2/7	2/7	2/7	2/7
Specific heat capacity, $c_p = R/\kappa$ ($10^4 \text{ J kg}^{-1} \text{K}^{-1}$)	1.26	1.41	1.10	1.12
Solar constant F_0 (W m^{-2})	50.7 ⁵	14.9 ⁵	3.71 ⁵	1.52 ⁵
Intrinsic heat flux (W m^{-2})	5.7 ⁶	2.01 ⁷	0.042 ⁷	0.433 ⁷
Bond albedo, r_∞	0.343 ⁸	0.342 ⁹	0.30 ³	0.29 ³
Single-scattering albedo, $\tilde{\omega}$	0.8	0.8	0.8	0.8
Solar optical depth, τ_{s0}	3.0	3.0	3.0	3.0
Thermal optical depth, τ_{l0}	80.0	120.0	60.0	40.0
Drag coefficient, k_0 (days^{-1})	1/100	1/100	1/100	1/100
No-drag latitude, ϕ_0	33°	33°	33°	33°
Horizontal resolution	T213	T213	T85	T85
Cut-off wavenumber for subgrid-scale dissipation	100	100	40	40

All parameter choices are constrained by knowledge of the physical properties of the planets and material properties of their atmospheres, as well as by observations where available. However, the drag formulation at the artificial lower boundary of the GCM is poorly constrained by data or physics. It represents the MHD drag the flow experiences in the interior of the planets.

In the interior of Jupiter and Saturn, the conductivity of molecular hydrogen increases with depth and becomes approximately constant where hydrogen becomes metallic at ~ 1.4 Mbar¹⁰. In the interior of Uranus and Neptune, the conductivity of the gas envelope likewise increases with depth and is determined by the conductivity of hydrogen and water ice¹¹. In the high-conductivity interior, the interaction of the magnetic field and the fluid flow produces Ohmic dissipation and retards the flow¹². In a deep atmosphere, this MHD drag affects the angular momentum balance averaged over cylinders concentric with the planet's spin axis¹. Since the drag only acts at great depth, the flow outside the cylinder tangent with the outermost region of substantial MHD drag is not affected by drag. Therefore, the flow in an equatorial latitude band in the upper atmosphere does not experience MHD drag.

We represented this MHD drag deep in the atmosphere in the simplest possible way in our thin-shell GCM, choosing the same drag formulation and depth of the artificial lower boundary in all giant planet simulations, to rule out that differences among them are caused by differences in

poorly constrained parameters. We chose the width of the no-drag region and the drag coefficient outside of it empirically, to obtain jets in the upper atmosphere that have similar strength and width as the observed jets. By choosing drag formulations that differ from planet to planet, better fits to observations could be obtained. The width of prograde equatorial jets, when they occur, depends weakly on the width of the no-drag region. For example, in a Jupiter simulation with a narrower no-drag region ($\phi_0 = 16^\circ$), the width of the equatorial jet is $\sim 5^\circ$ smaller than in the simulation reported here¹. The strength and width of off-equatorial jets depend weakly on the drag coefficient, with jets becoming stronger and wider as the drag coefficient is decreased, as seen in other simulations of geophysical turbulence^{1,13,14}. If the strength of the drag or the depth at which it acts is modified, the vertical shear of the zonal flow adjusts through “downward control” processes such that the angular momentum flux convergence or divergence integrated over atmospheric columns in a thin atmosphere (or over cylinders in a deep atmosphere) balances the drag on the zonal flow^{1,15,16}. However, neither the precise functional form of the drag (e.g., linear or quadratic in velocities), nor the magnitude of the drag coefficient where it is nonzero, nor the width of the no-drag region are essential for our results—as long as there is an equatorial region with no or sufficiently low drag such that a prograde jet can form^{1,17}.

2. Neptune control simulations

In Neptune’s atmosphere, eddies can be generated by (a) baroclinic instability off the equator induced by the differential solar heating, or (b) convective Rossby wave generation near the equator induced by the intrinsic heat flux. Eddies produced by these two mechanisms compete with each other in their contribution to the angular momentum transport to or from low latitudes. Since Neptune’s radius is smaller than that of Jupiter or Saturn, its meridional temperature gradients are generally larger, possibly increasing the importance of baroclinic eddy generation relative to convective Rossby wave generation. This may result in enhanced angular momentum flux divergence in low latitudes, counteracting any angular momentum convergence associated with convective Rossby wave generation. Feedbacks between eddies and the mean flow may contribute to preventing equatorial superrotation¹⁸. Indeed, a control simulation with Neptune’s physical parameters but with enhanced intrinsic heat flux (and thus an enhanced convective Rossby wave source) exhibits equatorial superrotation (Fig. S1, left column), as does a control simulation in which the global-mean insolation at the top of the atmosphere is unchanged but is imposed uniformly (so that baroclinic eddy generation is absent or strongly reduced) (Fig. S1, right column).

3. High-latitude vortices in the Jupiter and Saturn simulations

In high latitudes in the Jupiter and Saturn simulations, very large coherent vortices ($20^\circ \times 10^\circ$ longitude \times latitude) form spontaneously (Fig. S2). Since the coherent vortices preferentially exist in the region where absolute vorticity gradients vanish, and since the planetary vorticity gradient vanishes at the poles, formation of coherent vortices in high latitudes may require less vorticity mixing in the environment than it does at lower latitudes. Hence, the large coherent vortices in high latitudes may appear earlier in simulations. If the simulations were conducted for a longer period, large coherent vortices may also appear in lower latitudes, such as the latitude (23° S) of

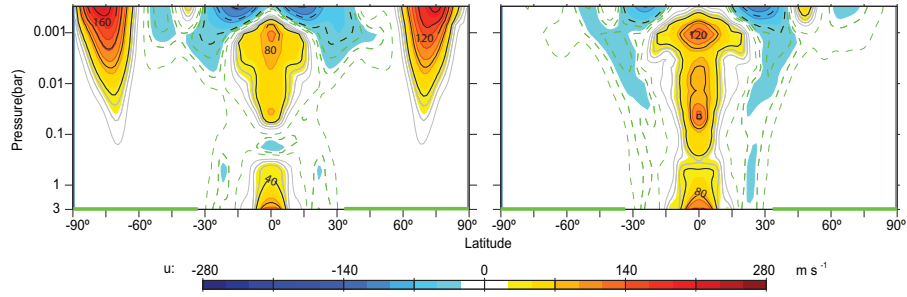


FIGURE S1: Mean zonal velocities in the latitude-pressure plane in Neptune control simulations. Contour intervals and colors as in Fig. 3. Left column: simulation with Neptune’s physical parameters but Saturn’s intrinsic heat flux (2.01 W m^{-2}). Right column: simulation with Neptune’s physical parameters but uniform insolation at the top of the atmosphere.

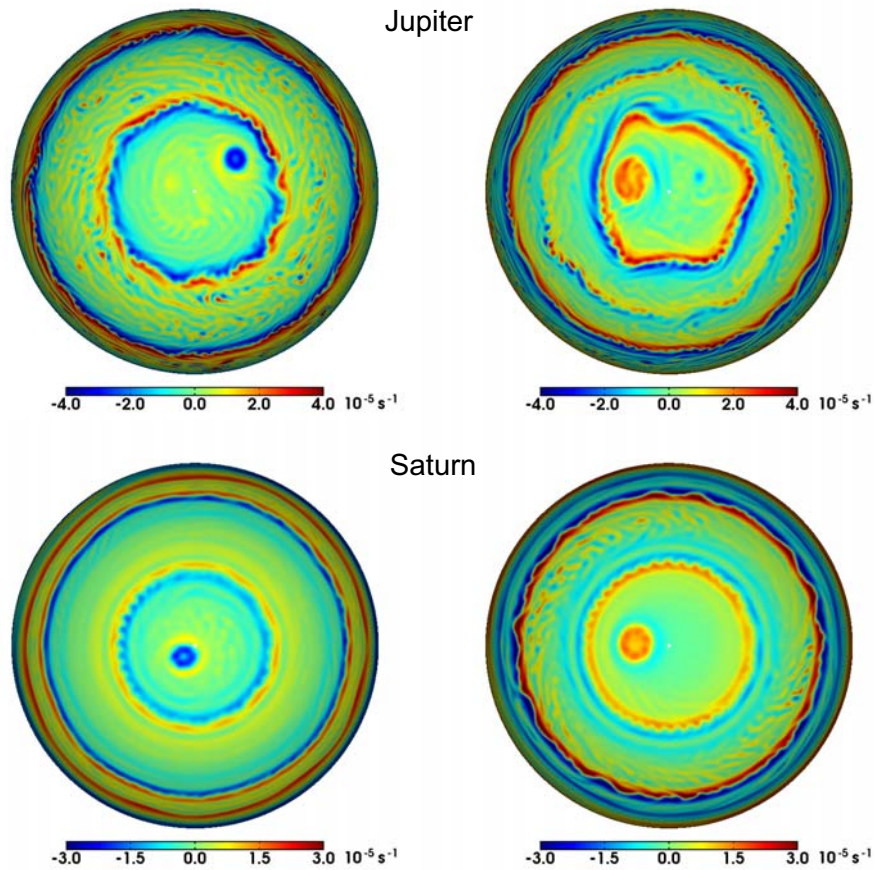


FIGURE S2: Vorticity in high latitudes in the Jupiter and Saturn simulations. Left column: south polar projection; right column: north polar projection.

the Great Red Spot on Jupiter (which is embedded in an environment of small absolute vorticity gradients^{19,20}).

The large coherent vortices are anticyclonic, with typical vorticities of magnitude $\sim 2 \times 10^{-5} \text{ s}^{-1}$. They are advected by the flow and maintain a temperature low in the center ($\sim 10 \text{ K}$ lower than the surroundings). These anticyclonic vortices are long-lived with life-spans determined by the radiative timescale. In the Jupiter simulation with an atmosphere of 3 bar thickness, the radiative timescale is ~ 10 Earth years; it is ~ 50 Earth years in the Saturn simulation. Since the radiative time scale increases with pressure, it is longer for deeper atmospheres, which might explain why the Great Red Spot on Jupiter is so long lived.

Supplementary References

1. Schneider, T. & Liu, J. Formation of jets and equatorial superrotation on Jupiter. *J. Atmos. Sci.* **66**, 579–601 (2009).
2. Guillot, T. A comparison of the interiors of Jupiter and Saturn. *Plan. Space Sci.* **47**, 1183–1200 (1999).
3. Lodders, K. & B. Fegley, J. *The Planetary Scientist's Companion* (Oxford University Press, 1998).
4. Donivan, F. F. & Carr, T. D. Jupiter's decameric rotation period. *Astrophys. J.* **157**, L65–L68 (1969).
5. Levine, J. S., Kraemer, D. R. & Kuhn, W. R. Solar-radiation incident on Mars and outer planets - latitudinal, seasonal, and atmospheric effects. *Icarus* **31**, 136–145 (1977).
6. Gierasch, P. J. *et al.* Observation of moist convection in Jupiter's atmosphere. *Nature* **403**, 628–630 (2000).
7. Guillot, T. The interiors of giant planets: Models and outstanding questions. *Ann. Rev. Earth Planet. Sci.* **33**, 493–530 (2005).
8. Hanel, R. A., Conrath, B. J., Herath, L. W., Kunde, V. G. & Pirraglia, J. A. Albedo, internal heat, and energy-balance of Jupiter - preliminary results of the Voyager infrared investigation. *J. Geophys. Res.* **86**, 8705–8712 (1981).
9. Hanel, R. A., Conrath, B. J., Kunde, V. G., Pearl, J. C. & Pirraglia, J. A. Albedo, internal heat flux, and energy balance of Saturn. *Icarus* **53**, 262–285 (1983).
10. Nellis, W. J., Weir, S. T. & Mitchell, A. C. Metallization and electrical conductivity of hydrogen in Jupiter. *Science* **273**, 936–938 (1996).
11. Nellis, W. J., Holmes, N. C., Mitchell, A. C., Hamilton, D. C. & Nicol, M. Equation of state and electrical conductivity of "synthetic Uranus," a mixture of water, ammonia, and isopropanol, at shock pressure up to 200 gpa (2 mbar). *J. Chem. Phys.* **107**, 9096–9100 (1997).
12. Liu, J. J., Goldreich, P. M. & Stevenson, D. J. Constraints on deep-seated zonal winds inside Jupiter and Saturn. *Icarus* **196**, 653–664 (2008).

13. Smith, K. S. *et al.* Turbulent diffusion in the geostrophic inverse cascade. *J. Fluid. Mech.* **469**, 13–48 (2002).
14. Danilov, S. & Gurarie, D. Rhines scale and spectra of the β -plane turbulence with bottom drag. *Phys. Rev. E* **65** (2002). Art. no. 067301.
15. Haynes, P. H., Marks, C. J., McIntyre, M. E., Shepherd, T. G. & Shine, K. P. On the downward control of extratropical diabatic circulations by eddy-induced mean zonal forces. *J. Atmos. Sci.* **48**, 651–679 (1991).
16. O’Gorman, P. A. & Schneider, T. Weather-layer dynamics of baroclinic eddies and multiple jets in an idealized general circulation model. *J. Atmos. Sci.* **65**, 524–535 (2008).
17. Scott, R. K. & Polvani, L. M. Equatorial superrotation in shallow atmospheres. *Geophys. Res. Lett.* **35**, L24202 (2008).
18. Saravanan, R. Equatorial superrotation and maintenance of the general circulation in two-level models. *J. Atmos. Sci.* **50**, 1211–1227 (1993).
19. Ingersoll, A. P. *et al.* Interaction of eddies and mean zonal flow on Jupiter as inferred from Voyager 1 and 2 images. *J. Geophys. Res.* **86**, 8733–8743 (1981).
20. Read, P. L. *et al.* Mapping potential-vorticity dynamics on Jupiter. I. Zonal-mean circulation from Cassini and Voyager 1 data. *Quart. J. Roy. Meteor. Soc.* **132**, 1577–1603 (2006).